Supporting Information

Coral-like directional porosity lithium ion battery cathodes by ice templating

Chun Huang and Patrick S. Grant

Department of Materials, University of Oxford, Parks Road, Oxford, OX1 3PH, UK

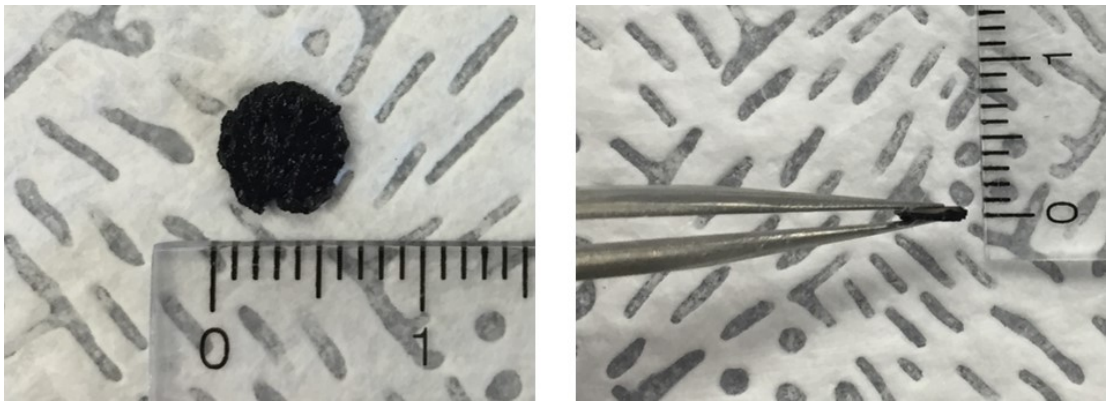

Figure S1: Photos of the $LiCoO_2$ (LCO) cathode by directional ice templating (DIT) that was dissembled from a battery cell after 200 charge and discharge cycles, demonstrating mechanical stability of the electrode.

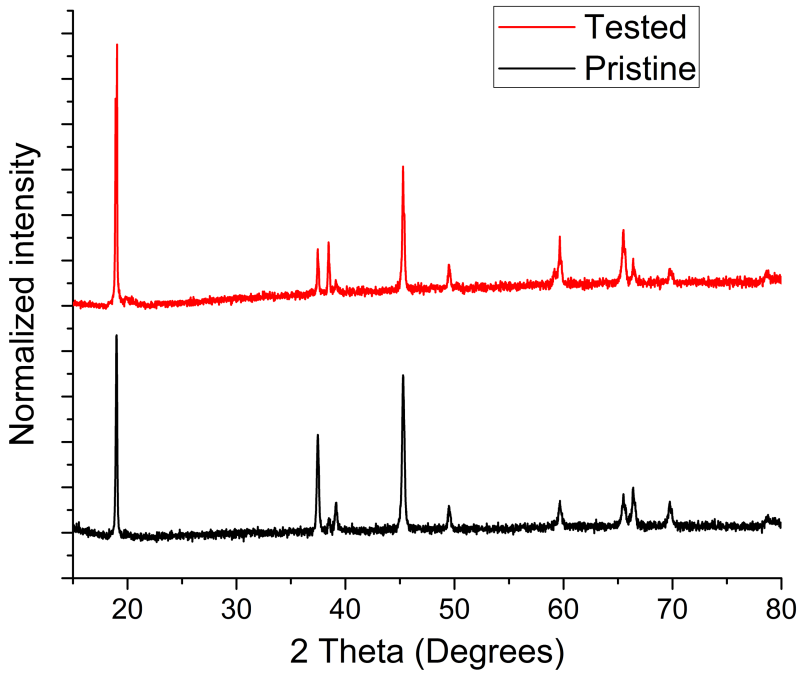

Figure S2: XRD patterns for the LCO electrode before and after 200 cycles of charge and discharge.

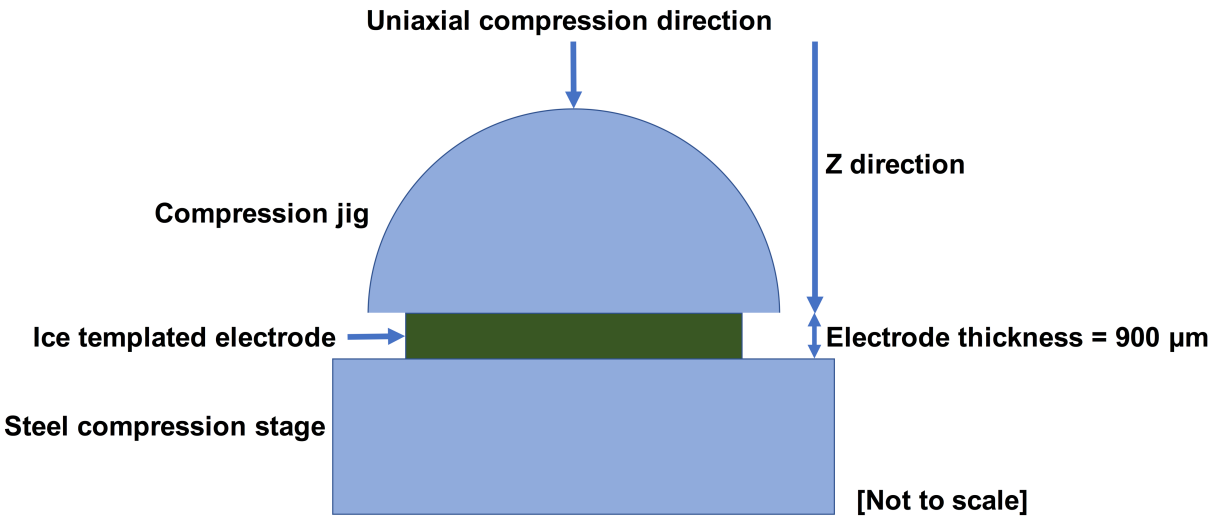

Figure S3: A schematic diagram to show the set-up for the compression testing of ice templated electrodes. The hemispherical compression jig was used to minimize compressive force misalignment and to provide a uniform compressive force on the electrode.

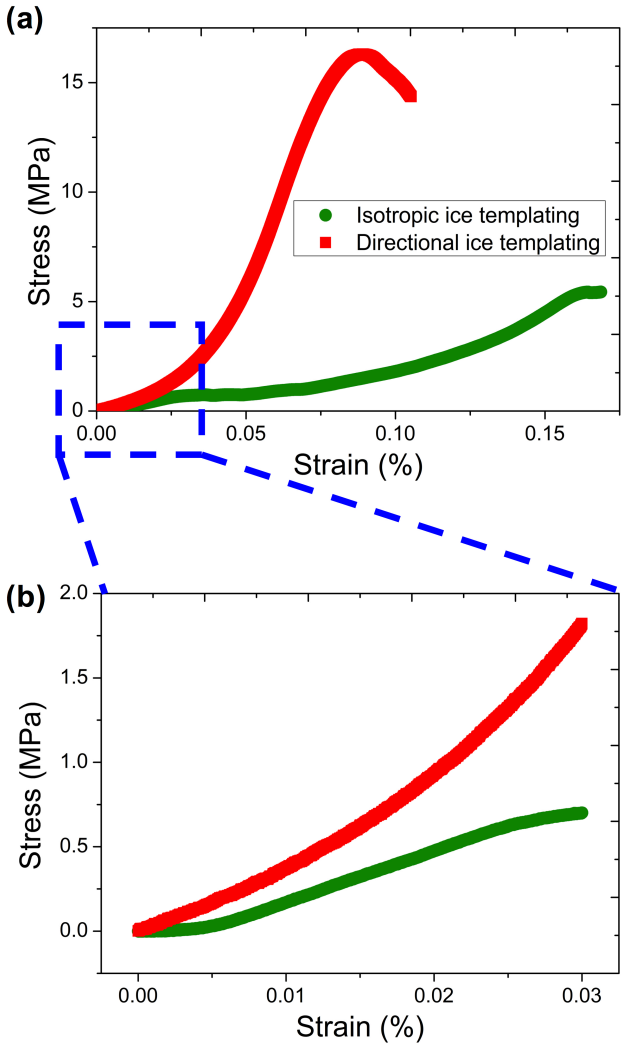

Figure S4: (a) Compressive stress-strain curves for the DIT and IIT electrodes; and (b) Zoom-in of the stress-strain curves at strains <0.03%.

With strains <0.03%, stress increased at a higher rate with strain for the DIT electrode than for the IIT electrode corresponding to a less compliant response in the through thickness direction for the aligned porosity structure. This region corresponds to localized buckling and micro-fracture along particle boundaries [R1]. At strains >0.03%, the gradual increase in stress of the isotropic structure indicated a slightly increased resistance to buckling and fracture: the gradual increase in stress reached an approximately steady strength of 5.4 MPa, indicative of a progressive structural collapse [R2-R3]. In contrast, stress increased at a higher rate with strain for the DIT electrode, due to the more structurally favourable orientation of the thick “pillars" of the coral-like structure with respect to the uniaxial compressive load [R4]. The DIT electrode exhibited a sudden structural collapse at a higher strength of 16.3 MPa.

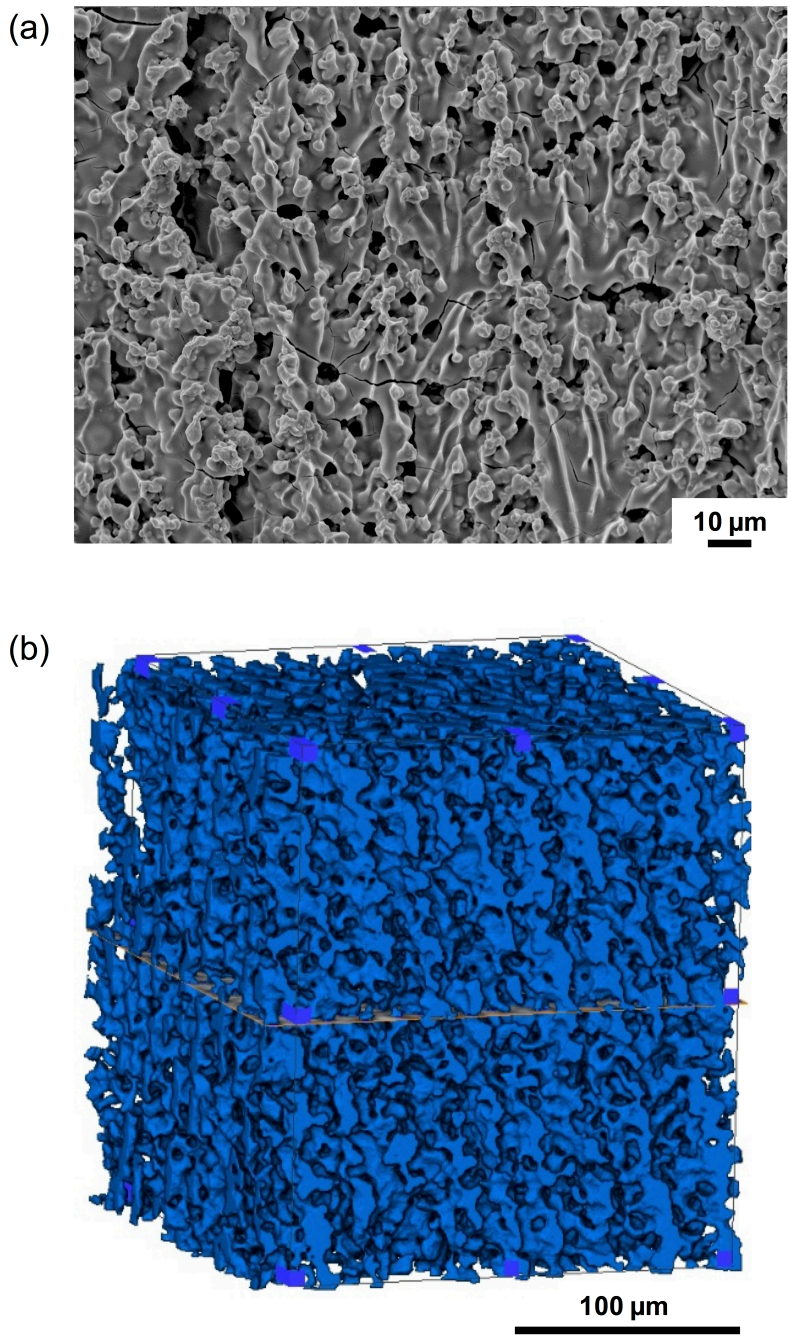

Figure S5: (a) Cross-sectional SEM image; and (b) 3D rendering by XCT of a DIT $LiCoO_2$ cathode that was made under a comparatively fast freezing rate of 0.5 K s^{-1}.

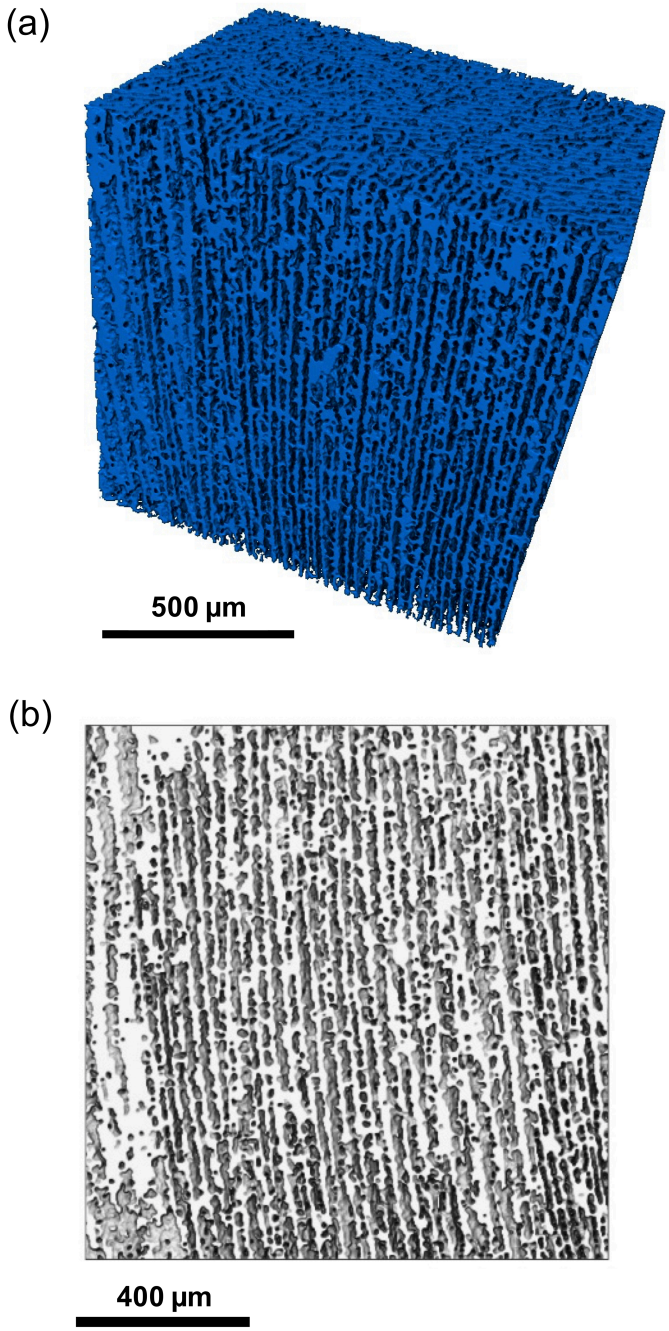

Figure S6: (a) 3D rendering; and (b) Cross-section 2D rendering by XCT of a DIT $LiNi_{0.8}Co_{0.15}Al_{0.05}O_2$ (NCA) cathode that was made under a freezing rate of 0.1 K s^{-1}.

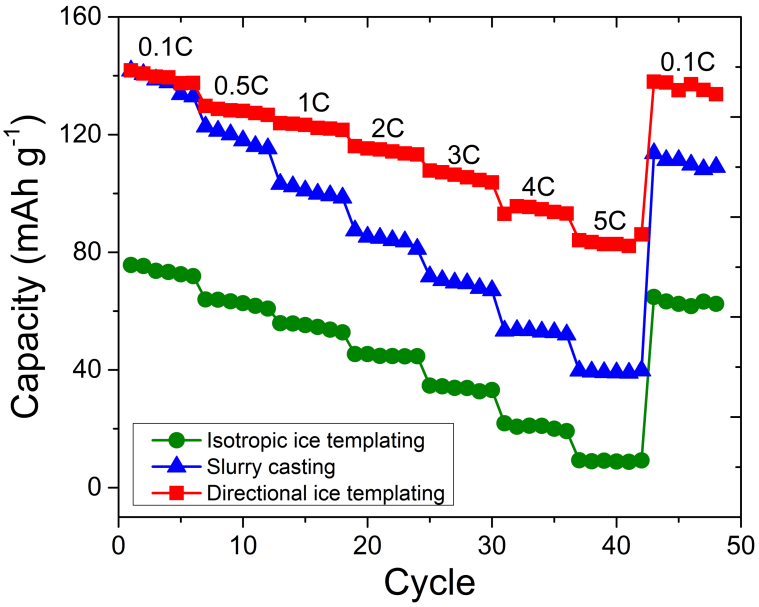

Figure S7: Reversible gravimetric capacities of the electrodes made by conventional slurry casting, isotropic and directional ice templating at different C rates.

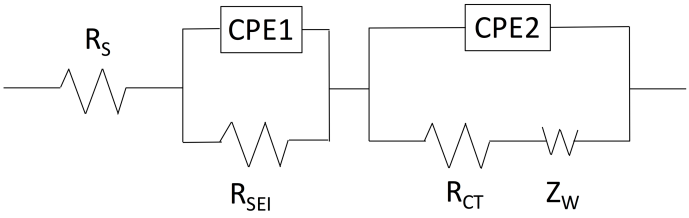

Figure S8: Equivalent circuit for the three types of electrode, where R_S is a series resistance that includes the electrical resistance of the electrode and the ionic resistance of the electrolyte, R_{SEI} is the resistance of current collector/electrode interface and the solid electrolyte interphase layer at the Li metal surface, *CPE1* is the corresponding constant phase element, R_{CT} is a charge transfer resistance that includes the charge transfer resistance of the electrode and the electrode/electrolyte interfacial resistance, *CPE2* is the corresponding constant phase element that is used for porous structures, and Z_W is a Warburg element corresponding to Li ion diffusion [R5,R6].

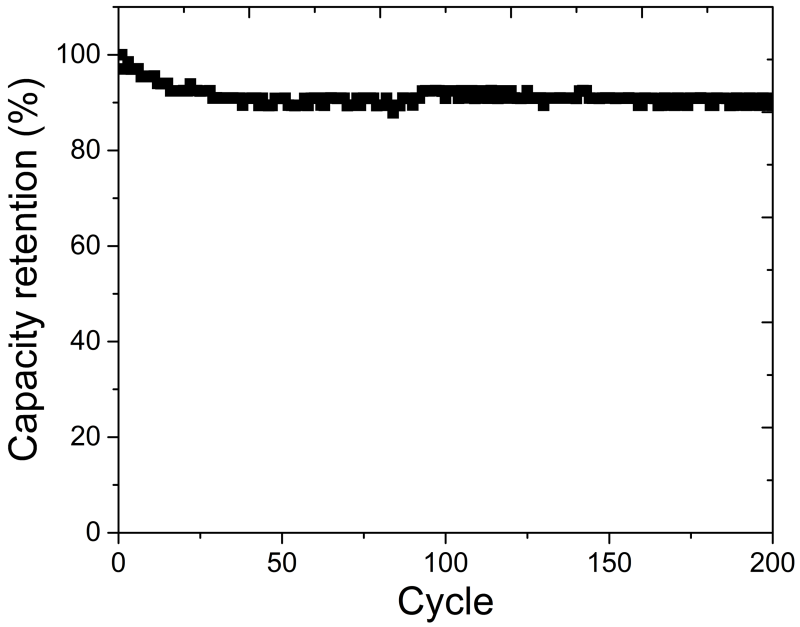

Figure S9: Reversible capacity retention for the DIT $LiCoO_2$ electrode as a function of cycle number at 1 C.

Calculation of energy and power densities based on cells

Following the method in [R7], because the weight and volume of packaging as well as the inactive edge of a cell depend on cell dimensions and configurations, we only consider elementary building blocks or units of LIBs. One unit of LIB comprises a cathode, a separator, a Li foil, ½ thickness cathode current collector (Al) and ½ thickness anode current collector (Cu). The estimated energy densities are for comparative purposes and do not reflect the practically attainable energy densities of battery full cells because practical anodes would be required. The reason for using ½ thickness current collectors is that the electrodes are usually coated on both sides of the current collectors in commercial LIBs. The parameters of the components used for the estimation are consistent with the relevant parameters in commercial LIBs [R7, R8].

In the same total volume, the proportions of inactive components in the LIB unit(s) are:

LIB unit(s) in the same total volume	vol.% inactive components	wt.% inactive components
1 LIB unit containing a DIT cathode	3.1	8.8
LIB units containing commercial SC cathodes	7.5	22.6

Table S1: vol.% and wt.% inactive components in both an LIB unit comprising a thick DIT LCO cathode, a separator, a lithium counter electrode and current collectors, and a stack of LIB units comprising commercial SC LCO cathodes, separators, lithium counter electrodes and current collectors, but of same total volume.

The gravimetric energy density E_g of the LIB unit(s) is calculated as [R9]:

$$E_g = Q_g V_{cell} M \quad (1)$$

where Q_g is the gravimetric capacity of the LIB, V_{cell} is the working voltage and M is the wt% of active components in LIB unit(s) of the same total volume.

The volumetric energy density E_v of the LIB unit(s) is calculated as:

$$E_v = Q_v V_{cell} N \quad (2)$$

where Q_v is the volumetric capacity of the LIB, V_{cell} is the working voltage and N is the vol.% of active components in LIB unit(s) of the same total volume.

The gravimetric power density P_g of the LIB unit(s) is calculated as [R10]:

$$P_g = E_g / t \quad (3)$$

where t is the duration of discharge at a specific C rate.

The volumetric power density P_v of the LIB unit(s) is calculated as:

$$P_v = E_v / t \quad (4)$$

Sample	Energy density		Power density		C rate
	Wh kg^{-1}	Wh L^{-1}	W kg^{-1}	W L^{-1}	h^{-1}
1 LIB unit containing a DIT cathode	435	509	395	463	1
	408	477	770	901	2
LIB units containing commercial SC cathodes	308	475	256	396	1
	260	402	473	732	2

Table S2: Energy and power densities for both an LIB unit comprising a thick DIT LCO cathode, a separator, a lithium counter electrode and current collectors, and a stack of LIB units comprising commercial SC LCO cathodes, separators, lithium counter electrodes and current collectors but of same total volume, at discharge rates of 1 and 2 C.

Component	Cost ($ kWh^{-1})	
	1 LIB unit containing a DIT cathode	LIB units containing commercial SC cathodes
Cu	5.8	14.0
Anode	12.9	20.1
Separator	26.7	64.8
Cathode	52.2	81.6
Al	0.6	1.4
Electrolyte	15.8	24.6
Pouch material	5.5	5.5
Tab material	1.3	1.3
Solvent	0.03	4.7
Solvent processing & drying	115.9	17.3
Solvent recovery	0	14.1
Total	236.5	249.4

Table S3: Costs for both an LIB unit comprising a thick DIT LCO cathode, a separator, a lithium counter electrode and current collectors, and a stack of LIB units comprising commercial SC LCO cathodes, separators, lithium counter electrodes and current collectors but of same total volume estimated at an energy density of 2C.

References

[R1] W.-J. Lai, M. Y. Ali and J. Pan, Mechanical behavior of representative volume elements of lithium-ion battery cells under compressive loading conditions, J. Power Sources 245 (2014) 609-623.

[R2] J. Seuba, S. Deville, C. Guizard and A. J. Stevenson, Mechanical properties and failure behavior of unidirectional porous ceramics, Sci. Reports 6:24326 **(**2016) DOI: 10.1038/srep24326.

[R3] S. Deville, E. Saiz, R. K. Nalla and A. P. Tomsia, Freezing as a path to build complex composites, Science 311 (2006) 515-518.

[R4] E. Munch, M. E. Launey, D. H. Alsem, E. Saiz, A. P. Tomsia, R. O. Ritchie, Tough, bio-inspired hybrid materials, Science 322 (2008) 1516-1520.

[R5] H. Manjunatha, K. C. Mahesh, G. S. Suresh and T. V. Venkatesha, The study of lithium ion de-insertion/insertion in $LiMn_2O_4$ and determination of kinetic parameters in aqueous Li_2SO_4 solution using electrochemical impedance spectroscopy, Electrochim. Acta 56 (3) (2011) 1439-1446.

[R6] N. Schweiker, R. Heinzmann, A. Eichhofer, H. Hahn and S. Indris, Electrochemical impedance spectroscopy of $Li_4Ti_5O_{12}$ and $LiCoO_2$ based half-cells and $Li_4Ti_5O_{12}$/$LiCoO_2$

cells: internal interfaces and influence of state-of-charge and cycle number, Solid State Ionics 226 (2012) 15-23.
[R7] F. Wu and G. Yushin, Conversion cathodes for rechargeable lithium and lithium-ion batteries, Energy Environ. Sci. 10 (2017) 435-459.
[R8] D. L. Wood III, J. Li and C. Daniel, Prospects for reducing the processing cost of lithium ion batteries, J. Power Sources 275 (2015) 234-242.
[R9] L.-L. Lu, Y.-Y. Lu, Z.-J. Xiao, T.-W. Zhang, F. Zhou, T. Ma, Y. Ni, H.-B. Yao, S.-H. Yu and Y. Cui, Wood-inspired high-performance ultrathick bulk battery electrodes, Adv. Mater. 1706745 (2018) 1-9.
[R10] W. Lai, C. K. Erdonmez, T. F. Marinis, C. K. Bjune, N. J. Dudney, F. Xu, R. Wartena and Y.-M. Chiang, Ultrahigh-energy-density microbatteries enabled by new electrode architecture and micropackaging design, Adv. Energy Mater. 22 (2010) E139-E144.